Susceptibility tensor imaging in the p-space without any rotation

Chunlei Liu[1,2] and Wei Li[1]

[1]*Brain Imaging and Analysis Center, Duke University, Durham, NC, United States,* [2]*Radiology, Duke University, Durham, NC, United States*

INTRODUCTION: Magnetic susceptibility anisotropy can be measured and characterized with the technique of susceptibility tensor imaging (STI) (1). While STI has provided a new way to study the microstructure of brain white matter and brain connectivity, the original experimental procedure requires rotation of the brain or the magnetic field. This requirement is challenging for routine imaging on standard scanners. In this study, we proposed and developed a novel method to measure multipole magnetic susceptibility anisotropy in a sub-voxel spectral space (**p**-space). This method of **p**-space STI measures higher-order frequency variations using a single image without rotating the object or the magnet. By sampling the **p**-space with pulsed field gradients or by shifted image reconstruction, we were able to measure a set of dipole and quadrupole susceptibility tensors. We illustrated the methodology in a simulation of aligned axons and demonstrated its use for 3D high-resolution imaging of fiber orientation in mouse brains *ex vivo* at 9.4 Tesla. We anticipate that the **p**-space approach may provide a powerful method for studying tissue microstructure and brain connectivity *in vivo* and non-invasively.

$$s(\mathbf{r}) = e^{-i2\pi\mathbf{p}\cdot\mathbf{r}} m(\mathbf{r},\mathbf{p}) e^{-i\Phi(\mathbf{r},\mathbf{p})} \quad [1]$$

$$\Phi(\mathbf{p}) = \Phi_0 + \gamma B_0 t\, \hat{\mathbf{p}}^T \chi_d \hat{\mathbf{p}} p + \gamma B_0 t\, \hat{\mathbf{p}}^T \chi_q \hat{\mathbf{p}} p^2 \quad [2]$$

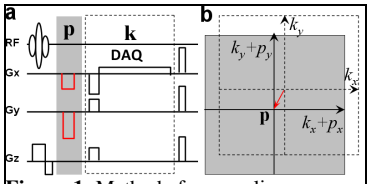

Figure 1. Methods for sampling **p**-space. (a) Spectral sensitizing gradients are applied before data acquisition in GRE. (b) This is equivalent to shifting **k**-space by a vector of **p**.

METHODS: Phase of gradient-echo images represents the amplitude of the mean field within a voxel. The spatial heterogeneity within a voxel, however, is not available. If the field distribution within a voxel can be recovered, it will allow us to infer the underlying tissue microstructure. One way to recover the field distribution is to apply an external magnetic field gradient which will modulate the resonance frequency of the spins within the voxel (Fig. 1). In the presence of a pulsed field-gradient **G**, the voxel-averaged MRI signal $s(\mathbf{r})$ at time t, ignoring T_2-relaxation, can be shown to be described by Eq. [1]. In a second-order multipole expansion, $\Phi(\mathbf{r},\mathbf{p})$ can be written as in Eq. [2]. In this equation, the first term is the mean phase. The second term is a dipole moment in which χ_d is a rank-2 dipole susceptibility tensor and $\hat{\mathbf{p}}$ is the unit directional vector. The third term is a quadrupole moment expressed in terms of a rank-2 quadrupole susceptibility tensor χ_q. More specifically, Φ_0 is the phase when no gradient is applied and it is related to the image-space dipole susceptibility tensor (rank 2) $\chi(\mathbf{r})$ following (1). The magnitude can be expanded similarly. Sampling the **p**-space can be achieved by applying a spectral sensitizing gradient vector (Fig. 1a), or equivalently by shifting **k**-space data (Fig. 1b).

A cubic voxel packed with an ensemble of parallel axons was generated. The voxel had a dimension of d = 256 μm on all sides. The axons were aligned along the z-axis. The B_0 field was parallel to the y-z plane, tilted by 50° from the z-axis (Fig. 2a). The inner radius of the axon was 3.5 μm and the outer radius was 5.0 μm. The distance between two neighboring axons was uniformly distributed between 11.0 μm and 12.5 μm. The susceptibility of the axons was set to be -0.082 ppm and the susceptibility anisotropy ($\chi_\parallel$ - $\chi_\perp$) of the myelin sheath was 0.163 ppm with $\chi_\parallel$being -0.1 ppm. Gaussian noise was added in the real and imaginary part of the signal resulting in an SNR of 20.

Adult 10-weeks old C57BL/6 mice were anesthetized and perfusion fixed. Images were acquired on a 9.4 T (400 MHz) 89-mm vertical bore Oxford magnet with shielded coil providing gradients of 2200 mT/m. The system is controlled by a GE EXCITE MR imaging console. A 3D spoiled-gradient-recalled-echo (SPGR) sequence was used with the following parameters: matrix size = 512x256x256, field-of-view (FOV) = 22x11x11 mm^3, bandwidth (BW) = 62.5 kHz, flip angle = 60º, TE = [4.4, 7.0, 9.0, 11.0, 13.0, 15.0] ms and TR = 100.0 ms.

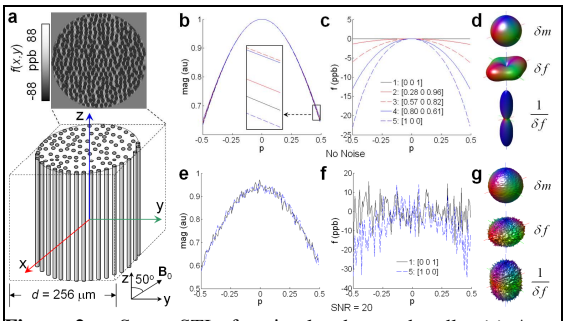

Figure 2. **p**-Space STI of a simulated axon bundle. (a) Axon structure and field distribution; (b-d) **p**-space signal without noise; (e-g) **p**-space signal with SNR = 20.

RESULTS: Fig. 2 shows results of the simulated bundle of parallel axons. Without noise, both magnitude and frequency showed a quadratic relationship with p as illustrated for five representative orientations (Fig. 2b&c), with frequency demonstrating clear anisotropy (Fig. 2c). We computed the standard deviation of the magnitude and phase along each direction. We further illustrated their anisotropic property with a set of 3D color-coded glyphs (Fig. 2d). For each point on the surface of the glyph, the radial distance from that point to the origin was proportional to the standard deviation for the corresponding radial direction. While the glyph of the magnitude appeared spherical (δm in Fig. 2d), the glyph of the frequency was donut-shaped (δf in Fib. 2d) with its inverse shaped like an elongated peanut ($1/\delta f$ in Fig. 2d). From these glyphs, the orientation of the axons is easily identified by searching for the minimal standard deviation. With SNR = 20, we observed similar behaviors even though significant fluctuations were present (Fig. 2e-g).

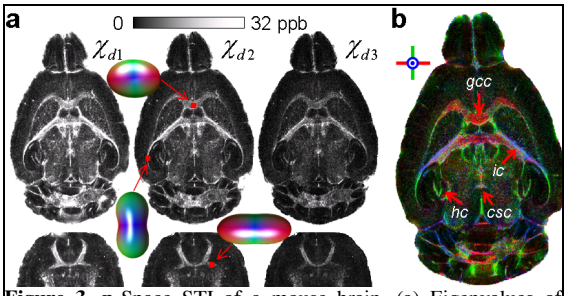

Figure 3. **p**-Space STI of a mouse brain. (a) Eigenvalues of dipole tensor; (b) color-coded minor eigenvector.

Fig. 3 shows representative results of the mouse brain reconstructed from a single image. Both the dipole and the quadrupole term showed clear anisotropy. Fig. 3a shows the three eigenvalues of the dipole susceptibility tensor with their 3D glyphs plotted for three voxels in major white matter fibers. All three glyphs demonstrated clear anisotropy and correctly identified the fiber orientation. Fig. 3b shows the color-coded minor eigenvector map with the intensity weighted by the trace. The orientations appeared to be consistent with the underlying axon orientation. For example, the genu of corpus callosum (gcc) appeared mainly red as it connects the right and left hemisphere. The laminated structure of the commissure of superior colliculus (csc) was clearly visible, interconnecting the superior colliculi on either side.

DISCUSSIONS AND CONCLUSIONS: We have proposed and demonstrated a method of **p**-space STI without any rotation. This method provides MRI a means to image higher order frequency information and utilize it to elucidate tissue microstructure. The method requires only a single acquisition of 3D GRE images. It also allows high spatial resolution. It does not involve rotating the object or the magnetic field. We expect the **p**-space method to open a new avenue for studying tissue microstructure in general and brain connectivity in particular.

With the **p**-space method, probing brain microstructure *in vivo* may become possible at resolutions higher than what current MRI methods are capable of. Higher field strength will further extend the ability of the method to quantify susceptibility anisotropy. Exploring the capability of the **p**-space method for imaging neuronal and muscular fiber connectivity could be of great interest for applications in which diffusion tensor imaging (DTI) (2) reaches its limits, such as imaging at high spatial resolution and at ultra-high field strength when tissue heating becomes problematic. In the future, **p**-space STI could be implemented to study moving organs such as kidneys, livers, fetus brains and even beating hearts as gradient echo can be easily gated and far less sensitive to motion.

REFERENCES: 1. Liu, C., MRM 63:1471-1477, 2010. 2. Basser P.J., et al, JMR B 103:247-254, 1994.